

# Towards Predicting Temporal Changes in a Patient’s Chest X-ray Images based on Electronic Health Records

Daemun Kyung<sup>1</sup>, Junu Kim<sup>1</sup>, Tackeun Kim<sup>2</sup>, Edward Choi<sup>1,†</sup>  
<sup>1</sup>KAIST, <sup>2</sup>TALOS Corp

**Abstract**—Chest X-ray imaging (CXR) is an important diagnostic tool used in hospitals to assess patient conditions and monitor changes over time. Generative models, specifically diffusion-based models, have shown promise in generating realistic synthetic X-rays. However, these models mainly focus on conditional generation using single-time-point data, *i.e.*, typically CXRs taken at a specific time with their corresponding reports, limiting their clinical utility, particularly for capturing temporal changes. To address this limitation, we propose a novel framework, EHRXDiff, which predicts future CXR images by integrating previous CXRs with subsequent medical events, *e.g.*, prescriptions, lab measures, etc. Our framework dynamically tracks and predicts disease progression based on a latent diffusion model, conditioned on the previous CXR image and a history of medical events. We comprehensively evaluate the performance of our framework across three key aspects, including clinical consistency, demographic consistency, and visual realism. We demonstrate that our framework generates high-quality, realistic future images that capture potential temporal changes, suggesting its potential for further development as a clinical simulation tool. This could offer valuable insights for patient monitoring and treatment planning in the medical field.

**Index Terms**—CXR generation, Medical records, Diffusion model.

## I. INTRODUCTION

Chest X-ray imaging (CXR) is a crucial diagnostic tool employed in hospitals to evaluate a patient’s health status and to track changes over time. Due to its cost-efficiency and low radiation dose, CXR is the most frequently performed imaging technique in hospitals. This widespread use makes building large-scale datasets relatively easy compared to other medical imaging methods, leading many studies to focus on training AI models using these X-ray datasets. However, existing datasets often suffer from issues such as class imbalances and noisy labels.

Generative models offer the potential to address these challenges by generating CXRs depicting specific diseases or modeling desired pathology locations and severity. The recent success of high-quality image generation in the general domain has inspired studies to create realistic synthetic CXRs in the medical field. Initial efforts [1]–[3] used Generative Adversarial Networks (GANs) [4] or VQ-VAE [5], which were state-of-the-art (SOTA) models for image generation. Recently, stable diffusion [6] models like RoentGAN [7] and Cheff [8] have been explored to generate high-fidelity medical images.

Existing CXR generation models primarily focus on generating images with under-represented labels using conditional generation based on CXR labels [1], [2] or paired CXR reports [3], [7]–[10]. However, these methods are limited to synthesizing realistic CXRs at a single time point and cannot provide future images of specific patients. Thus, they only serve as data augmentation tools for addressing class imbalances, without leveraging the capability of CXRs to track the progression of a patient’s condition over time. Given that CXR imaging is crucial not only for assessing current health status but also for monitoring disease progression, a new framework that incorporates temporal changes is needed.

Recently, BiomedJourney [11] proposed a counterfactual medical image generation framework. Given two CXR reports taken at different

time points for a specific patient, GPT-4 is used to synthesize the disease progression between the two CXRs. Then, BiomedJourney generates high-quality counterfactual images by using the first CXR image and the progression description from the text. However, this approach serves a different purpose, since it is not considering the temporal progression of patient status (*i.e.*, generating the most likely future CXRs), but rather generating CXRs given an arbitrary progression scenario (*e.g.*, what would the patient’s CXR look like if he was to develop a new nodule?).

Electronic Health Records (EHRs) are large-scale multimodal databases that encompass a patient’s comprehensive medical history, including structured records such as diagnoses, procedures, and medications, along with imaging modalities like chest X-rays (CXR). Given the multimodal nature of EHRs, and the fact that doctors in clinical practice rely on both patient images and EHR tabular data for the decision-making process [12], [13], it is natural as well as potentially useful to predict changes in a patient’s condition by combining previous images with subsequent medical history.

In this paper, we introduce a novel task focused on predicting future CXRs by combining previous CXRs with subsequent events from the EHR table data, and present EHRXDiff, the first latent diffusion-based model to perform this task. This approach offers a dynamic view of a patient’s temporal changes, tracking their condition based on medical events such as medication or treatment starting from the initial status of the patient (*i.e.*, the previous CXR image). We comprehensively evaluate the quality of the predicted CXRs of our proposed model. Specifically, our framework shows potential as a simulation tool for healthcare professionals by outperforming baselines in tracking patients’ changing states over time.

## II. METHODOLOGY

### A. Task Definition

Given the previous CXR image  $I_{prev}$  and a sequence of medical events  $\mathcal{S}_{event} = (e_1, e_2, \dots, e_{n_{event}})$ , the model predicts the target CXR image  $I_{trg}$ . We work with the triple  $(I_{prev}, \mathcal{S}_{event}, I_{trg})$ , where  $I_{prev}, I_{trg} \in \mathbb{R}^{3 \times H \times W}$ , and  $\mathcal{S}_{event}$  consists of table events  $e_i$  (*e.g.*, prescriptions, lab tests) occurring at time  $t_i$  between the two imaging times. Here,  $H$  and  $W$  are the input image resolution, and  $i \in \{1, \dots, n_{event}\}$ , with  $n_{event}$  indicating the total number of events. Our approach is more challenging than the previous works [7], [8], [10] since it incorporates the patient’s medical history rather than relying on simple text descriptions. The model must recognize the initial state from the previous image and predict the patient’s status based on the provided history.

### B. Encoder Modules for CXR and Medical events Integration

To predict future CXR images based on previous CXR images and consecutive medical events, the model must (1) produce realistic, high-quality CXR images and (2) accurately reflect the potential clinical status based on prior images and medical histories. To achieve this, the framework includes three encoders: a VAE encoder, and two CLIP

<sup>†</sup> Corresponding author

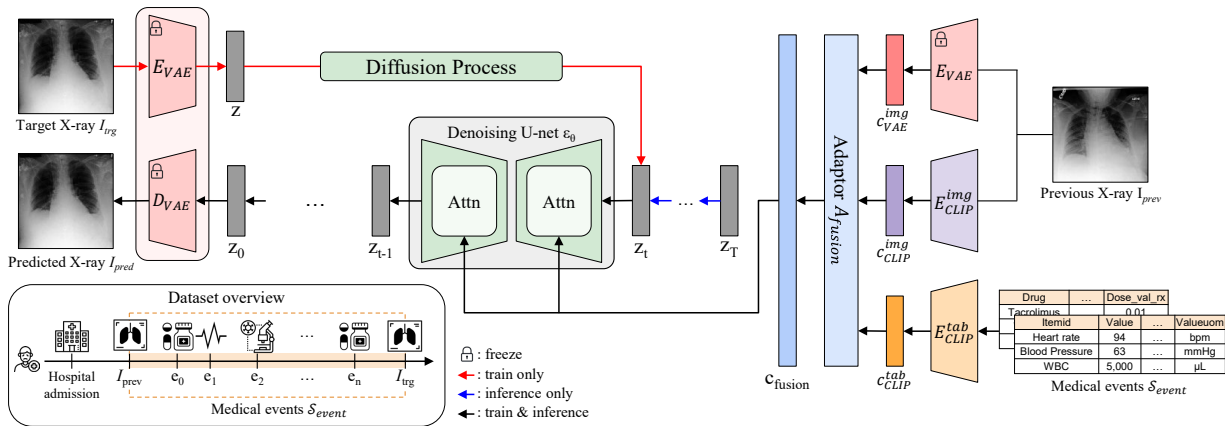


Fig. 1. Overall framework. During training, a random timestep  $t$  is sampled, and the latent vector  $z$  is corrupted to  $z_t$  via diffusion process. For inference, Gaussian noise is sampled and iteratively denoised over  $T$  steps. In both cases, image embeddings from CLIP and VAE encoders ( $E_{CLIP}^{img}$ ,  $E_{VAE}$ ) and table embeddings from CLIP table encoder ( $E_{CLIP}^{tab}$ ) are fused by an Adaptor module to condition the denoising U-Net.

TABLE I  
OVERALL STATISTICS OF OUR DATASET.

	train	valid	test
# of patients	9,295	595	407
# of hospital admission ids	11,263	730	523
# of samples ( $I_{prev}$ , $S_{event}$ , $I_{trg}$ )	101,819	5,654	5,596
avg. time interval per sample (hours)	25.64	25.87	25.84

encoders for each of the image and table modalities. The outputs from these encoders are then integrated using an adaptor module, efficiently leveraging both the previous images and medical events. Details of each module are provided below.

The VAE encoder,  $E_{VAE}$ , captures fine-grained visual details such as the shapes of major organs (e.g., lungs and heart) and the locations and sizes of lesions, which are crucial for understanding and preserving the structural information of input CXR images. We denote the VAE embedding of the previous CXR image as  $c_{VAE}^{img} \in \mathbb{R}^{C_z \times H_f \times W_f}$ , where  $C_z$  represents the number of channels of latent vector, and  $H_f$  and  $W_f$  represent the height and width of the feature map, respectively.

We use separate CLIP encoders for two modalities: the image CLIP encoder ( $E_{CLIP}^{img}$ ) and the table CLIP encoder ( $E_{CLIP}^{tab}$ ). These encoders are pre-trained on pairs of previous CXR images and associated medical events ( $I_{prev}$ ,  $S_{event}$ ). The  $E_{CLIP}^{img}$  extracts high-level clinical features related to the patient’s initial clinical status from  $I_{prev}$ , while the  $E_{CLIP}^{tab}$  captures relevant information from medical events, effectively interpreting the patient’s medical history and its impact on their condition. We extract the CLIP embedding  $c_{CLIP}^{img} \in \mathbb{R}^{n_{patch} \times D_{CLIP}}$  and  $c_{CLIP}^{tab} \in \mathbb{R}^{n_{event} \times D_{CLIP}}$  from the input CXR and medical events sequences, respectively. Here,  $n_{patch}$  refers to the number of visual patches from the Vision Transformer (ViT) encoder [14],  $n_{event}$  refers to the number of tabular events, and  $D_{CLIP}$  represents the dimension of the CLIP features.

The adaptor module ( $A_{fusion}$ ) merges the embeddings of the VAE and CLIP encoders, combining the fine-grained details from the VAE with the high-level clinical features captured by CLIP. This fusion allows the model to predict future CXR images that not only represent the structural and clinical nuances from the input images, but also reflect potential temporal changes based on medical events. Given that the VAE embedding  $c_{VAE}^{img}$  has a 2D feature map per channel and the CLIP embeddings are 1D per token, we first flatten  $c_{VAE}^{img}$  and

TABLE II  
QUANTITATIVE RESULTS FOR MEDICAL INFORMATION PRESERVATION ON THE TEST SET. (MEAN  $\pm$  STD)

	Chest Imagenome (weighted macro AUC)		
	all	diff	same
GT	0.842	0.722	0.905
Previous image	0.798	0.558	0.902
Previous label	0.672	0.000	1.000
Table Classifier	0.611	0.502	0.661
Table Classifier (w/ prev label)	0.693	0.106	0.981
EHRXDdiff	0.722 $\pm$ 0.003	0.576 $\pm$ 0.005	0.796 $\pm$ 0.003
EHRXDdiff <sub>w_null</sub>	0.764 $\pm$ 0.004	0.580 $\pm$ 0.008	0.844 $\pm$ 0.004

project it to match the dimensionality of the CLIP feature. We then concatenate all the features and fuse them using a linear layer. The resulting fused feature is  $c_{fusion} \in \mathbb{R}^{C_{fusion} \times D_{CLIP}}$ , where  $C_{fusion}$  refers to the number of channels in the fused feature.

In previous works [6], [11], [15], the image condition is often concatenated with the input noise of the denoising U-Net. This approach works well for tasks like image-to-image translation or super-resolution, where the output needs to be spatially aligned with the input image. However, for CXR image pairs, even consecutive images may not be perfectly aligned due to factors like patient posture or breathing [16]. Thus, our task requires integrating diverse information from prior CXR images rather than replicating structural details. To achieve this, we replace the concatenation strategy with a cross-attention mechanism using an adaptor module as described above. This approach enables the model to focus on meaningful changes rather than preserving strict spatial alignment.

### C. Diffusion Models for EHR based CXR prediction

We use the state-of-the-art image generation model, Latent Diffusion Model (LDM) [6], as our backbone. The LDM consists of the following two components: 1) Variational autoencoder (VAE) with encoder  $E_{VAE}$  and decoder  $D_{VAE}$ , which projects the image to a lower-dimensional latent representation  $z$  and then reconstructs the image from  $z$ . 2) Conditional denoising U-Net  $\epsilon_\theta$  that iteratively denoises an initially randomly generated latent vector. The objective function of a text-conditioned LDM is defined as:

$$\mathcal{L}_{LDM} = \mathbb{E}_{z_t \sim \mathcal{N}(0,1), t} \left[ \|\epsilon_t - \epsilon_\theta(z_t, t, c_{text})\|_2^2 \right] \quad (1)$$

where  $\epsilon_\theta$  is a time-conditional denoising U-net that predicts the noise  $\epsilon_t$  added to the latent representation  $z_t \in \mathbb{R}^{C_z \times H_f \times W_f}$  at time  $t \in \{1, \dots, T\}$ , and  $c_{\text{text}}$  is the text description embedding. Our framework modifies this objective function to predict the target image  $I_{\text{Irg}}$  based on the previous image  $I_{\text{prev}}$  and consecutive table events  $S_{\text{event}}$ . The modified objective function is:

$$\mathcal{L}_{\text{ours}} = \mathbb{E}_{z_t \sim \mathcal{N}(0,1), t} \left[ \|\epsilon_t - \epsilon_\theta(z_t, t, c_{\text{fusion}})\|_2^2 \right] \quad (2)$$

where  $c_{\text{fusion}}$  is the condition embedding that combines the table and previous image, as describe in Section II-B, while other aspects remain the same as above.

### D. Dataset

We extracted  $(I_{\text{prev}}, S_{\text{event}}, I_{\text{Irg}})$  triples from the MIMIC-IV [17] and MIMIC-CXR [18] datasets. MIMIC-CXR is the only publicly available imaging resource that can be linked to MIMIC-IV (EHR tabular data), making it ideal for constructing our dataset\*. We selected seven core event types describing the temporal progression of patient status: lab results, input events, charts output events, prescriptions, procedures, and microbiology results.

EHR records capture all events that occur during a hospital stay, with patients often experiencing thousands of events per day, especially during stays in the intensive care unit (ICU) [19]. This abundance of data makes it a challenge for the model to identify and utilize important information. Therefore, we focus on cardiovascular and lung-related items from the EHR tables that could affect CXR images. This item selection was manually validated by a medical expert. We converted the tabular events into free-text format, such as “*table\_name column1 value1 ...*,” following Hur *et al.* [20]. Each event  $e_i$  was then converted into an embedding vector using OpenAI’s embedding model (text-embedding-ada-002). For images, we used only frontal view (PA, AP) images and selected patients with at least two CXR images during hospitalization. We focused on CXR pairs that occurred within a maximum of two days to exclude outliers, considering model input size limitations and the observation that around 80% of consecutive CXR images are taken within this time frame. Detailed statistics are provided in Table I.

To help the model learn correlations within our triplets, we introduce an additional technique that adds a sample  $(I_{\text{prev}}, S_{\text{null}}, I'_{\text{prev}})$  where  $I_{\text{prev}}$  and  $I'_{\text{prev}}$  represent the same CXR image with different augmentations, and  $S_{\text{null}}$  represents an empty set of table events. The augmentation of  $I_{\text{prev}}$  to create  $I'_{\text{prev}}$  involves weak transformations such as rotation or scaling, which simulate patient movements during imaging while preserving all clinically relevant information. This approach teaches the model to maintain consistency in clinical findings when there are no significant events in the EHR table. These samples help the model distinguish between clinically significant changes and insignificant variations.

## III. EXPERIMENTS

### A. Experimental Settings

**Implementation Details.** We implemented our LDM model based on Weber *et al.* [8]. We used a VAE encoder pretrained with MaCheX [8]. For the CLIP encoder, we employed ViT-B/32 [14] for images and a 2-layer transformer encoder for tables. The table transformer is configured with a maximum input length of 1024, a feature dimension of 1536, and 24 attention heads. The input image resolution is  $256 \times 256$ . We set  $C_z$ ,  $H_f$ , and  $W_f$  to 3, 64, and 64,

\*Both datasets are publicly accessible through the PhysioNet platform (<https://physionet.org/>)

TABLE III

QUANTITATIVE RESULTS FOR IMAGE QUALITY AND DEMOGRAPHIC PRESERVATION ON THE TEST SET. (MEAN  $\pm$  STD)

	FID ( $\downarrow$ )	Age ( $\uparrow$ ) (Pearson corr.)	Gender ( $\uparrow$ ) (AUROC)
GT	-	0.719	0.995
Previous image	0.16	0.740	0.996
EHRXDiff	$5.98_{\pm 0.07}$	$0.453_{\pm 0.007}$	$0.963_{\pm 0.002}$
EHRXDiff <sub>w_null</sub>	$4.57_{\pm 0.07}$	$0.554_{\pm 0.012}$	$0.979_{\pm 0.001}$

TABLE IV

QUANTITATIVE RESULT OF DIFFERENT CONDITIONING INPUT FOR OUR MODEL ON THE TEST SET. (MEAN  $\pm$  STD)

concat	crossattn			Chest Imagenome (weighted macro AUC)		
$E_{\text{VAE}}$	$E_{\text{VAE}}$	$E_{\text{CLIP}}^{\text{img}}$	$E_{\text{CLIP}}^{\text{tab}}$	all	diff	same
✓				$0.646_{\pm 0.001}$	$0.536_{\pm 0.007}$	$0.709_{\pm 0.002}$
	✓			$0.621_{\pm 0.001}$	$0.537_{\pm 0.026}$	$0.674_{\pm 0.008}$
		✓		$0.746_{\pm 0.004}$	$0.567_{\pm 0.007}$	$0.836_{\pm 0.010}$
			✓	$0.624_{\pm 0.003}$	$0.549_{\pm 0.007}$	$0.661_{\pm 0.010}$
✓			✓	$0.660_{\pm 0.009}$	$0.586_{\pm 0.018}$	$0.701_{\pm 0.011}$
✓		✓	✓	$0.725_{\pm 0.001}$	$0.569_{\pm 0.008}$	$0.797_{\pm 0.006}$
	✓	✓	✓	$0.722_{\pm 0.003}$	$0.576_{\pm 0.005}$	$0.796_{\pm 0.003}$

respectively. The dimension  $D_{\text{CLIP}}$  is 768, and  $n_{\text{patch}}$  is 65. We set  $C_{\text{fusion}}$  to 1024. Each model was trained for 100 epochs with a batch size of 128 (1024 for CLIP pre-training). We used the AdamW [21] optimizer with an initial learning rate of  $5e-4$  for CLIP pre-training and  $5e-5$  for LDM training. All models were implemented in PyTorch [22] and trained on an RTX A6000 GPU. Due to the stochastic nature of diffusion model inference, we predict the output 3 times using different random seeds and report the mean and standard deviation for each metric.

**Evaluation Metrics.** We evaluate the quality of the predicted X-rays using three categories of metrics: preservation of medical information, preservation of demographic information, and image quality. To assess the preservation of medical information, we use multi-label CXR pathology classifier based on Chest ImaGenome labels [23]. Specifically, we fine-tune a pre-trained ViT model on MIMIC-CXR following Bae *et al.* [24], using our training set. We focus on the 10 most frequent Chest ImaGenome labels with a prevalence between 0.05 and 0.95. To assess the preservation of demographic information, we use classifiers for gender and age, applying state-of-the-art classifiers for age [25], while gender is evaluated by fine-tuning the XRV DenseNet-121 [26] classifier on our training set. To assess image quality, we calculate the Fréchet Inception Distance (FID) score [27] using DenseNet-121 trained on multiple CXR datasets [28].

**Baselines.** Since our work is the first to predict temporal CXR images using previous images and tabular data, there is no existing baseline model for a direct comparison. Therefore, we define four baselines: the *previous image*, the *previous label*, the *table classifier*, and the *table classifier (w/ prev label)*. The *previous image* baseline simply uses  $I_{\text{prev}}$  as the predicted image, representing a scenario where only the previous image is used without attempting to predict temporal changes. This baseline can serve as a potential shortcut for the future CXR prediction model. However, due to the inherent uncertainty in the classifier, it does not output exactly 0 or 1, even for images with ground truth labels of 0 or 1. To eliminate this uncertainty, we introduce the *previous label* baseline, which directly compares the GT label of  $I_{\text{prev}}$  with that of  $I_{\text{Irg}}$ , instead of relying on the classifier’s output. Our framework is designed to not only predict future CXR pathology labels but also to represent them as natural CXR images.

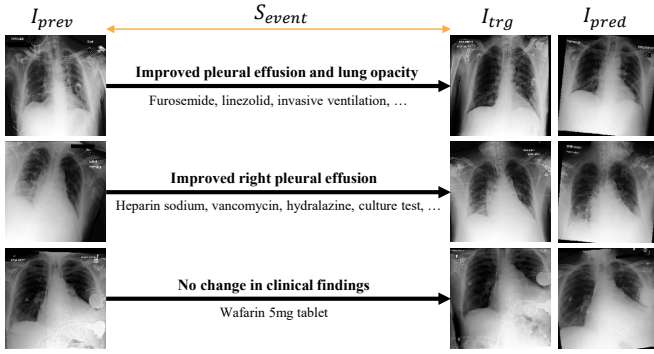


Fig. 2. Qualitative results.  $I_{prev}$  and  $I_{trg}$  are real CXR images from two different timestamps, while  $I_{pred}$  is predicted by EHRXDiff<sub>w<sub>null</sub></sub>.  $S_{event}$  (below the arrows) represents the medical events between the two timepoints, with **Bold** indicating descriptions of the differences between the CXRs.

To evaluate model performance without the complexity of generating CXR images, we propose a new baseline called the *table classifier*, which directly predicts CXR pathology labels based on tabular data. This baseline has two versions: one with previous label information and one without it. We fine-tune our CLIP table encoder,  $E_{CLIP}^{tab}$  by adding a linear layer for multi-label prediction. In the version that uses previous label information (*table classifier (w/ prev label)*), we concatenate a learnable label embedding of the previous CXR image’s GT label to the input. We use label embeddings instead of prior image embeddings to simplify the interpretation of the previous image’s label, as this baseline aims to assess model performance under the simplest possible conditions.

## B. Results

**Preservation of medical info.** In Table II, we compare the CXR pathology classification performance of EHRXDiff and EHRXDiff<sub>w<sub>null</sub></sub> models with four baseline models defined in Section III-A, using weighted macro AUROC on the Chest ImaGenome test set. We analyze the results in three categories: the *all* category reflects the overall performance on the entire test set, while the *same* and *diff* categories refer to the test subsets where the labels for  $I_{prev}$  and  $I_{trg}$  are identical or different, respectively. Both of our models share the same architecture (Fig. 1), but EHRXDiff<sub>w<sub>null</sub></sub> additionally uses the augmentation technique described in Section II-D.

For the *all* category, we compare only the *table classifier* and *table classifier (w/ prev label)* with our models, as *previous image* and *previous label* set the upper and lower bounds for the *same* and *diff* subset, making overall performance comparisons unfair. Our models outperform the *table classifier* variants, even though they only predict multi-label outputs without generating a CXR image. Additionally, *table classifier (w/ prev label)* tends to overfit by exploiting shortcuts to replicate the input label. These results show that using table input alone limits CXR pathology prediction due to the lack of visual context, while incorporating image data instead of simple labels reduces the risk of shortcut-based overfitting by providing richer, more diverse information.

For *diff* category, our models outperform all baselines, achieving approximately 80% AUROC compared to the GT. This suggests that our models effectively leverage medical history to track temporal changes in clinical findings. However, performance in the *diff* subset is generally lower than in the *same* subset even for the GT. We hypothesize that this discrepancy may be due to rapid status changes (e.g., within 2 days), which can place patients in a “borderline”, making accurate predictions more challenging.

In the *same* category, our models outperform the *table classifier* but underperform compared to *table classifier (w/ prev label)*, as the latter simply replicates the previous label. EHRXDiff<sub>w<sub>null</sub></sub> outperforms EHRXDiff thanks to its augmentation technique, which helps the model avoid altering clinical findings when there are no significant events in the medical history. As a result, EHRXDiff<sub>w<sub>null</sub></sub> achieves a 93% AUROC in the *same* subset compared to the GT, demonstrating that our model successfully recognizes when the patient’s status remains unchanged with high performance.

**Preservation of demographic info.** We show the performance regarding demographic preservation in Table III. While we successfully maintain gender information, we encounter limitations in preserving accurate age data. This suggests that gender cues are more easily detectable in the input images, whereas predicting precise age from CXR images remains a challenging task.

**Image Fidelity and Qualitative Results.** In Table III, the EHRXDiff and EHRXDiff<sub>w<sub>null</sub></sub> models achieve low FID scores, compared to SOTA text-conditional CXR generation models [7] with scores ranging from 3 to 9. This demonstrates their ability to generate realistic, high-quality CXR images, as also shown in Fig. 2. EHRXDiff<sub>w<sub>null</sub></sub> effectively captures temporal changes, such as resolving the white appearance in the left lung in both  $I_{trg}$  and  $I_{pred}$  in rows 1-2, while preserving the overall status in row 3. However, there are limitations in maintaining finer details. For example, our model detects only one device, missing the other in row 3.

**Ablation Study.** We analyze the effectiveness of our conditioning inputs by comparing test set performance in Table IV. Rows 1-4 illustrate the impact of various conditioning methods. Rows 1 and 2 use the same VAE embedding, but differ in how it is fed into the model: concatenation with the U-Net input or cross-attention via attention layers of U-Net. When using only image conditions (rows 1-3), we observe high performance in the *same* subset. The CLIP embedding outperforms the VAE embedding due to its high-level features, which are more directly related to CXR pathology. However, this approach has limitations in the *diff* subset. With only table embeddings (row 4), the model struggles due to the lack of visual context. In rows 5-6, we concatenate the VAE embedding with the U-Net input while using attention layers to cross-attend to the CLIP embedding, similar to Instruct-Pix2Pix [15]. In row 7, all features are integrated into the LDM using cross-attention. The results indicate that the CLIP embeddings provide complementary information to the model (rows 5-6), and combining all features (row 7) improves performance in a *diff* subset by effectively leveraging information from multiple source. Since row 7 demonstrates the best performance in the *diff* subset, which is important to capturing the temporal state changes, while maintaining comparable performance in the *same* subset, we select it as our model architecture.

## IV. CONCLUSION

In this paper, we introduce EHRXDiff, a novel framework designed to predict future CXR images by integrating previous CXRs with subsequent medical events. We comprehensively validate EHRXDiff’s performance, demonstrating its potential to capture temporal changes in CXR findings, as well as its ability to generate high-quality, realistic CXR images. These findings suggest the potential for further development as a clinical simulation tool, providing valuable insights for patient monitoring and treatment planning in the medical field. However, there is still room for improvement compared to the GT, especially in retaining fine-grained details. In future work, we aim to improve performance through more precise feature sampling guided by medical experts or by incorporating other modalities, such as text.

## REFERENCES

- [1] Mohamed Loey, Florentin Smarandache, and Nour Eldeen M. Khalifa, "Within the lack of chest covid-19 x-ray dataset: A novel detection model based on gan and deep transfer learning," *Symmetry*, vol. 12, no. 4, 2020.
- [2] Shobhita Sundaram and Neha Hulkund, "Gan-based data augmentation for chest x-ray classification," in *KDD Applied Data Science for Healthcare Workshop*, 2021.
- [3] Hyungyung Lee, Da Young Lee, Wonjae Kim, Jin-Hwa Kim, Tackeun Kim, Jihang Kim, Leonard Sunwoo, and Edward Choi, "Vision-language generative model for view-specific chest x-ray generation," in *CHIL*, 2024.
- [4] Ian Goodfellow, Jean Pouget-Abadie, Mehdi Mirza, Bing Xu, David Warde-Farley, Sherjil Ozair, Aaron Courville, and Yoshua Bengio, "Generative adversarial nets," in *Advances in Neural Information Processing Systems*, 2014.
- [5] Aaron van den Oord, Oriol Vinyals, and koray kavukcuoglu, "Neural discrete representation learning," in *Advances in Neural Information Processing Systems*, 2017.
- [6] Robin Rombach, Andreas Blattmann, Dominik Lorenz, Patrick Esser, and Björn Ommer, "High-resolution image synthesis with latent diffusion models," in *CVPR*, 2022.
- [7] Pierre Chambon, Christian Bluethgen, Jean-Benoit Delbrouck, Rogier Van der Sluijs, Małgorzata Połacin, Juan Manuel Zambrano Chaves, Tanishq Mathew Abraham, Shivanshu Purohit, Curtis P. Langlotz, and Akshay Chaudhari, "Roentgen: Vision-language foundation model for chest x-ray generation," in *arXiv*, 2022.
- [8] Tobias Weber, Michael Ingrisch, Bernd Bischl, and David Rügamer, "Cascaded latent diffusion models for high-resolution chest x-ray synthesis," in *PAKDD*, 2023.
- [9] Junjie Shentu and Noura Al Moubayed, "Cxr-irgen: An integrated vision and language model for the generation of clinically accurate chest x-ray image-report pairs," in *WACV*, 2024.
- [10] Pierre Joseph Marcel Chambon, Christian Bluethgen, Curtis Langlotz, and Akshay Chaudhari, "Adapting pretrained vision-language foundational models to medical imaging domains," in *NeurIPS 2022 Foundation Models for Decision Making Workshop*, 2022.
- [11] Yu Gu, Jianwei Yang, Naoto Usuyama, Chunyuan Li, Sheng Zhang, Matthew P. Lungren, Jianfeng Gao, and Hoifung Poon, "Biomedjourney: Counterfactual biomedical image generation by instruction-learning from multimodal patient journeys," in *arXiv*, 2023.
- [12] Shih-Cheng Huang, Anuj Pareek, Saeed Seyyedi, Imon Banerjee, and Matthew P Lungren, "Fusion of medical imaging and electronic health records using deep learning: a systematic review and implementation guidelines," in *npj Digital Medicine*, 2020.
- [13] V.E. Kerchberger, J.A. Bastarache, C.M. Shaver, J.B. McNeil, C.T. Wang, N.S. Zheng, A. Tapdiya, W.-Q. Wei, and L.B. Ware, "Chest radiograph interpretation is critical for identifying acute respiratory distress syndrome patients from electronic health record data," in *American Journal of Respiratory and Critical Care Medicine*, 2020.
- [14] Alexey Dosovitskiy, Lucas Beyer, Alexander Kolesnikov, Dirk Weissenborn, Xiaohua Zhai, Thomas Unterthiner, Mostafa Dehghani, Matthias Minderer, Georg Heigold, Sylvain Gelly, Jakob Uszkoreit, and Neil Houlsby, "An image is worth 16x16 words: Transformers for image recognition at scale," in *ICLR*, 2021.
- [15] Tim Brooks, Aleksander Holynski, and Alexei A. Efros, "Instructpix2pix: Learning to follow image editing instructions," in *CVPR*, 2023.
- [16] Giridhar Dasegowda, Mannudeep K. Kalra, Alain S. Abi-Ghanem, Chiara D. Arru, Monica Bernardo, Luca Saba, Doris Segota, Zhale Tabrizi, Sanjaya Viswamitra, Parisa Kaviani, Lina Karout, and Keith J. Dreyer, "Suboptimal chest radiography and artificial intelligence: The problem and the solution," in *Diagnostics*, 2023.
- [17] Alistair E. W. Johnson, Lucas Bulgarelli, Lu Shen, Alvin Gayles, Ayad Shammout, Steven Horng, Tom J. Pollard, Sicheng Hao, Benjamin Moody, Brian Gow, Li-wei H. Lehman, Leo A. Celi, and Roger G. Mark, "Mimiciv, a freely accessible electronic health record dataset," *Scientific data*, 2023.
- [18] Alistair E. W. Johnson, Tom J. Pollard, Seth J. Berkowitz, Nathaniel R. Greenbaum, Matthew P. Lungren, Chih-ying Deng, Roger G. Mark, and Steven Horng, "Mimic-cxr, a de-identified publicly available database of chest radiographs with free-text reports," *Scientific data*, 2019.
- [19] L Nelson Sanchez-Pinto, Yuan Luo, and Matthew M Churpek, "Big data and data science in critical care," in *Chest*, 2018.
- [20] Kyunghoon Hur, Jungwoo Oh, Junu Kim, Jiyouon Kim, Min Jae Lee, Eunbyeol Cho, Seong-Eun Moon, Young-Hak Kim, Louis Atallah, and Edward Choi, "Genhpf: General healthcare predictive framework for multi-task multi-source learning," in *IEEE Journal of Biomedical and Health Informatics*, 2024.
- [21] Ilya Loshchilov and Frank Hutter, "Decoupled weight decay regularization," in *ICLR*, 2019.
- [22] Adam Paszke, Sam Gross, Francisco Massa, Adam Lerer, James Bradbury, Gregory Chanan, Trevor Killeen, Zeming Lin, Natalia Gimelshein, Luca Antiga, Alban Desmaison, Andreas Köpf, Edward Z. Yang, Zach DeVito, Martin Raison, Alykhan Tejani, Sasank Chilamkurthy, Benoit Steiner, Lu Fang, Junjie Bai, and Soumith Chintala, "Pytorch: An imperative style, high-performance deep learning library," in *NeurIPS*, 2019.
- [23] Joy T. Wu, Nkechinyere N. Agu, Ismini Lourentzou, Arjun Sharma, Joseph A. Paguio, Jasper S. Yao, Edward C. Dee, William Mitchell, Satyananda Kashyap, Andrea Giovannini, Leo A. Celi, and Mehdi Moradi, "Chest imagenome dataset for clinical reasoning," in *NeurIPS Datasets and Benchmarks Track (Round 2)*, 2021.
- [24] Seongsu Bae, Daecun Kyung, Jaehyeon Ryu, Eunbyeol Cho, Gyubok Lee, Sunjun Kwon, Jungwoo Oh, Lei Ji, Eric I-Chao Chang, Tackeun Kim, and Edward Choi, "Ehrxqa: A multi-modal question answering dataset for electronic health records with chest x-ray images," in *NeurIPS 2023 Datasets and Benchmarks Track*, 2023.
- [25] Hirotaka Ieki, Kaoru Ito, Mike Saji, Rei Kawakami, Yuji Nagatomo, Kaori Takada, Toshiya Kariyasu, Haruhiko Machida, Satoshi Koyama, Hiroki Yoshida, Ryo Kurosawa, Hiroshi Matsunaga, Kazuo Miyazawa, Kouichi Ozaki, Yoshihiro Onouchi, Susumu Katsushika, Ryo Matsuoka, Hiroki Shinohara, Toshihiro Yamaguchi, Satoshi Kodera, Yasutomi Higashikuni, Katsuhito Fujii, Hiroshi Akazawa, Nobuo Iguchi, Mitsuaki Isobe, Tsutomu Yoshikawa, and Issei Komuro, "Deep learning-based age estimation from chest x-rays indicates cardiovascular prognosis," in *Communications Medicine*, 2022.
- [26] Joseph Paul Cohen, Joseph D. Viviano, Paul Bertin, Paul Morrison, Parsa Torabian, Matteo Guarrera, Matthew P Lungren, Akshay Chaudhari, Rupert Brooks, Mohammad Hashir, and Hadrien Bertrand, "TorchXRVision: A library of chest X-ray datasets and models," in *Medical Imaging with Deep Learning*, 2022.
- [27] Martin Heusel, Hubert Ramsauer, Thomas Unterthiner, Bernhard Nessler, and Sepp Hochreiter, "Gans trained by a two time-scale update rule converge to a local nash equilibrium," in *Neural Information Processing Systems*, 2017.
- [28] Joseph Paul Cohen, Mohammad Hashir, Rupert Brooks, and Hadrien Bertrand, "On the limits of cross-domain generalization in automated x-ray prediction," in *Medical Imaging with Deep Learning*, 2020.